9-21-2022

Development of an End-Effector Type Therapeutic Robot with Sliding Mode Control for Upper-Limb Rehabilitation

Md Mahafuzur Khan

Asif Al Zubayer Swapnil

Tanvir Ahmed

Md Mahbubur Rahman

Md Rasedul Islam

See next page for additional authors

Authors

Md Mahafuzur Khan, Asif Al Zubayer Swapnil, Tanvir Ahmed, Md Mahbubur Rahman, Md Rasedul Islam, Brahim Brahmi, Raouf Fareh, and Mohammad Habib Rahman

robotics

MDPI

Article

Development of an End-Effector Type Therapeutic Robot with Sliding Mode Control for Upper-Limb Rehabilitation

Md Mahafuzur Rahaman Khan [1], Asif Al Zubayer Swapnil [1], Tanvir Ahmed [2], Md Mahbubur Rahman [1], Md Rasedul Islam [3], Brahim Brahmi [4,*], Raouf Fareh [5] and Mohammad Habibur Rahman [1]

1 Department of Mechanical Engineering, University of Wisconsin-Milwaukee, Milwaukee, WI 53211, USA
2 Biomedical Engineering, University of Wisconsin-Milwaukee, Milwaukee, WI 53211, USA
3 Richard. J Resch School of Engineering, University of Wisconsin—Green Bay (UWGB), Green Bay, WI 54311, USA
4 Electrical Engineering Department, College Ahuntsic, Montreal, QC H2M 1Y8, Canada
5 Electrical Engineering Department, University of Sharjah, Sharjah P. O. Box 27272, United Arab Emirates
* Correspondence: brahim.brahmi@collegeahuntsic.qc.ca

Abstract: Geriatric disorders, strokes, spinal cord injuries, trauma, and workplace injuries are all prominent causes of upper limb disability. A two-degrees-of-freedom (DoFs) end-effector type robot, iTbot (intelligent therapeutic robot) was designed to provide upper limb rehabilitation therapy. The non-linear control of iTbot utilizing modified sliding mode control (SMC) is presented in this paper. The chattering produced by a conventional SMC is undesirable for this type of robotic application because it damages the mechanical structure and causes discomfort to the robot user. In contrast to conventional SMC, our proposed method reduces chattering and provides excellent dynamic tracking performance, allowing rapid convergence of the system trajectory to its equilibrium point. The performance of the developed robot and controller was evaluated by tracking trajectories corresponding to conventional passive arm movement exercises, including several joints. According to the results of experiment, the iTbot demonstrated the ability to follow the desired trajectories effectively.

Keywords: upper-limb rehabilitation; end-effector robot (iTbot); sliding mode control; reaching law; trajectory tracking

Citation: Khan, M.M.R.; Swapnil, A.A.Z.; Ahmed, T.; Rahman, M.M.; Islam, M.R.; Brahmi, B.; Fareh, R.; Rahman, M.H. Development of an End-Effector Type Therapeutic Robot with Sliding Mode Control for Upper-Limb Rehabilitation. *Robotics* **2022**, *11*, 98. https://doi.org/10.3390/robotics11050098

Academic Editor: Raffaele Di Gregorio

Received: 27 July 2022
Accepted: 15 September 2022
Published: 21 September 2022

1. Introduction

Globally, approximately 15 million individuals suffer from neurological diseases, such as strokes. This total comprises one-third fatalities and about an equal number of patients who spend the rest of their lives with irreversible disability [1]. In the USA, approximately 750,000 persons are affected by stroke [2], leaving most survivors with varying degrees of motor dysfunction [3]. Stroke is the third most significant cause of disabilities globally [4]. Approximately 85 % of stroke survivors who suffer from hemiparesis live with acute arm impairment [5]. As a result, 60% of individuals with upper limb hemiparesis experience long-term functional limitations, which reduces their quality of life [6,7]. This poor life quality includes losing the ability to work and failing to self-care. These consequences have a significant social and economic impact on the families of those affected and society [8,9]. The recovery of function of the upper limb can play a significant role in reinstating quality of life. Robots are able to assist in recovery from upper and lower limb dysfunction arising from neurological disorders, as reported in several recent studies [10–13].

Traditional rehabilitation focuses on rehabilitative exercises, in which the patient performs a series of bodily motions under the guidance of a trained therapist. A number of researchers have set their sights on developing medical rehabilitation devices [14]. Robot-aided rehabilitation provides high-intensity therapy and decreases the workload of medical staff, unlike traditional rehabilitative treatment. Additionally, this modern therapy can

facilitate the quantitative recording of data related to the recovery progress. Robots can provide passive, active, and active-assistive therapies for impaired limbs [15,16].

In general, upper limb robotic devices are subdivided into two types: end-effector type and exoskeleton type robots [17]. Exoskeleton robots are designed to be worn on human limbs [18–20]. The design of this type of robot mimics human anatomical joints and the length of limb segments. Due to the multiple "bundling" of the exoskeleton robot and the upper limbs, the patient cannot detach from the robot quickly if unexpected danger occurs [21]. Many exoskeleton robots can provide rehabilitation therapy for full arm motion and rehabilitation therapy in passive and active modes and provide endpoint-based therapy [22–25]. However, these exoskeleton robots are frequently costly, cumbersome, structurally complicated, and lack mobility. In contrast, end-effector type rehabilitation robots are designed to attach to users at a single point, usually at the wrist or forearm. The primary advantage of end-effector type devices over exoskeletons is their simplicity in design and manufacture. End-effector robots are more compact and lightweight than other robots, and they are easier to build. Furthermore, because of the single-point interaction between the two entities, end-effector type devices are the most prevalent type of assistive device [26–28]. An end-effector-type robot is easy to install in a patient's home because of its simple structure and presents a low risk.

The control techniques used for therapeutic devices directly impact the success of robotic rehabilitation training. Patients with acute hemiplegia can benefit from a patient-passive training program, which requires the afflicted limb to reach a specified trajectory while passively executing repetitive movements [29]. The rehabilitation training system is more complicated than traditional manipulators due to the robot's highly non-linear dynamics, unknown external disturbances, and the viscoelastic features of biological joints [30]. In order to improve position control during repetitive reach training, rehabilitation robots have been designed that use a variety of control methods, such as adaptive control [31], flatness-based control [32], EMG-based control [33], admittance control [34], fuzzy and backstepping control [35]. Sliding mode control (SMC) is an effective technique for controlling robotic systems with unknown dynamics and constrained disturbances [36]. Theoretically, SMC's robustness guarantees optimal tracking performance regardless of parameter or model uncertainty [37]. Furthermore, SMC has a simple construction, strong transient performance, and rapid response. As a result, we evaluate SMC as a viable option for providing reliable, high-quality tracking in dynamic environments. The control input that carries the switching function signum (sign(.)) is the primary source of issues in conventional SMC [38]. In real-time implementation, this function's switching results in undesired chattering due to the control effort. Therefore, the system's performance degrades, and unmodeled high-frequency dynamics may be triggered. Islam et al. [39] proposed a unique upper limb exoskeleton with sliding mode fractional control (FSMC), due to its excellent tracking performance and durability against external disturbances. Using this method, the suggested controller's settling time and maximum pitch angle control were enhanced. Furthermore, in comparison to traditional SMC, tracking and chatter were found to be enhanced. Babaiasl et al. [40] introduced SMC to a three DoFs exoskeleton for shoulder joint rehabilitation, using a genetic algorithm to modify the SMC parameters. They found that SMC performed well in this non-linear control process and that uncertainties and disturbances (such as patients' hand tremors) were effectively rejected. Rahman et al. [29] developed a rehabilitative exoskeleton for the lateral side of the upper limb with non-linear SMC to aid in rehabilitation and improve upper-limb movement. In the device developed, they combined the concept of a saturation (sat) function [41] with an ERL [42] to implement trajectory tracking. The authors utilized a non-linear SMC approach to move the ETS-MARSE so that it could deliver a variety of passive rehabilitation activities, including single-joint movement exercises and workouts involving the movement of multiple joints. This enabled the controller to regulate the exoskeleton's movement, allowing it to conduct passive rehabilitation treatment.

Therefore, the goal of the present investigation was to develop a novel sliding mode controller (SMC) reaching law capable of quickly converging a system trajectory to an equilibrium point. In the proposed approach, fast convergence does not provoke any chattering as occurs with conventional sliding mode controllers. The proposed approach utilizes adjustable parameters so that the control law applied significantly reduces the unwanted chattering phenomenon. Furthermore, the designed approach can provide a faster convergence time than the exponential reaching law, which is among the best solutions to avoid chattering problems and produce a fast convergence time.

The remainder of the article is organized as follows. Section 2 provides an overview of the iTbot. In Section 3, the iTbot's kinematics and dynamics are discussed. Section 4 presents the control design and stability analysis. The experimental findings and a comparative study assessment are reported in Section 5. Finally, Section 6 presents the conclusions and suggestions for future work.

2. Overview of the iTbot

The iTbot was developed based on the human reachable workspace to provide therapy covering the full range of the workspace. Figure 1, depicts the structural design of the iTbot, which was designed to be a minimally feasible solution for a functional robot-aided rehabilitation treatment system.

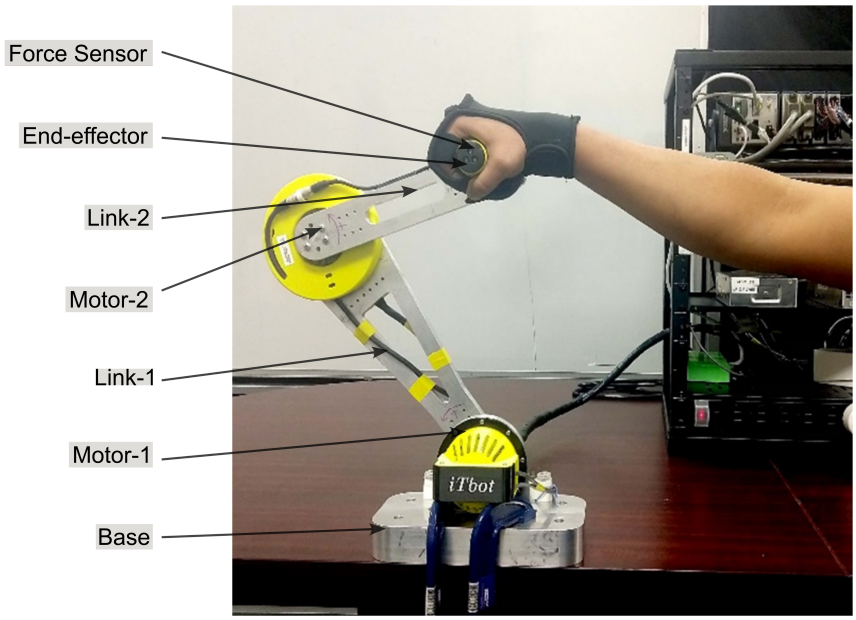

Figure 1. Mechanical design of the iTbot.

The body of the iTbot is made up of the base, as well as two linkages (Link-1 and Link-2). The robot's base contains two fabricated aluminum parts, one being the bottom base of the robot, and the other a mounting for the Motor-1 (Joint-1) hardware shown in Figure 1. The base is designed as a heavy aluminum block to provide stability during the robot's operation during experiments. It also carries a plastic bumper with rubber stoppers to stop the robot at the limit of its range of motion. The Joint-1 (Motor-1) consists of a harmonic drive gear reducer mounted directly on the top base part, with the motor mounted on its back with a custom-designed motor adapter. Link-1, which consists of an aluminum portion with a gear reducer mounted directly to it, is directly connected to the harmonic drive gear reduction unit's output. In the Link-2 assembly, the fabricated aluminum part contains the second half of the Motor-2 wire spool holder. The Joint-2 (Motor-2) is composed of two links (Link-1 and Link-2). There is an end-effector at the end of the connection, which holds the force sensor and the handle. The handle is custom-designed to match the user's hand profile; in our prototype, the average size of the two

adult male laboratory members who participated in the development of the iTbot. The handle has a base part, 3D-printed in polycarbonate plastic, that mounts on the force sensor. An inner tube with mounting features for two bearings on both ends is used—this tube screws into the base part.

Specification of the iTbot

The completed CAD model was created by assigning materials to each component in SolidWorks software. The developed iTbot's parameters are listed in Table 1 below.

Table 1. Mechanical parameters of iTbot estimated from CAD model.

Joint Parameters		
Item	Joint-1	Joint-2
Joint range of motion (Degrees)	±85°	±180°
Link Parameters		
Mass (Kg)	1.79	0.65
Location of the center of gravity in link frame (m)	Center of gravity of link 1 in frame {1} X_1= 0.26, Y_1= 0.00, Z_1 = 0.00	Center of gravity of link 2 in frame {2} X_2= 0.15, Y_2= 0.00, Z_2 = 0.02
Robot Properties		
Mass (Kg)	6.67 (3.2 without base)	
Maximum horizontal reach (m)	±0.55	
Maximum vertical reach (m)	+0.1 to +0.55	

In the X-axis configuration, the iTbot can provide a 1.1 m range of motion. It can achieve the design goal of supporting human upper limb motion [43] in the desired workspace [44,45] fitting any patients with a height from 1.21 m to 1.82 m for the horizontal and vertical configurations shown in Figure 2. In the shaded region from Figure 2, a human arm is covered from 0.5 m to 0.66 m. However, the iTbot symmetric design with asymmetric joint range of motion makes it proficient for ambidextrous use. The base design allows both positionings either in horizontal or vertical orientation.

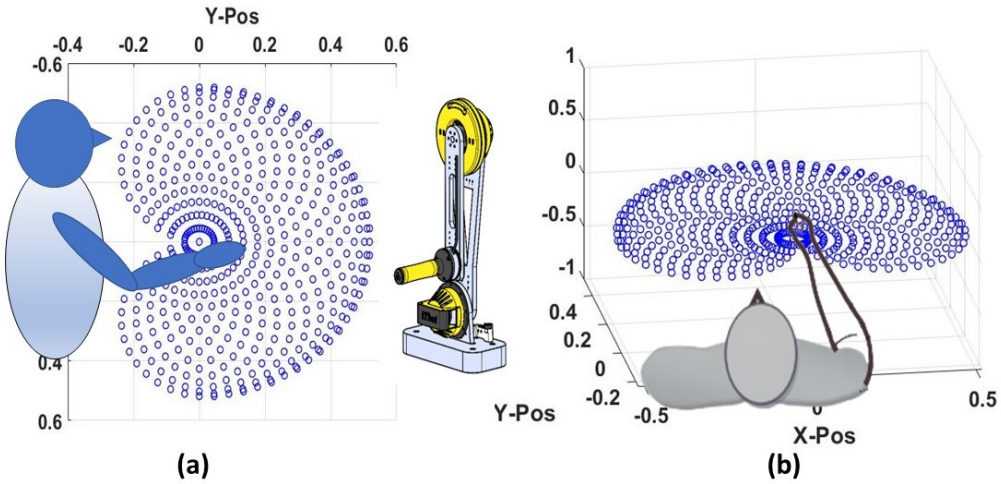

Figure 2. Workspace of the upper limb for (**a**) vertical and (**b**) horizontal configuration.

3. Description of Kinematics and Dynamics of iTbot

3.1. Kinematics of the iTbot

As shown in Figure 3, only the two joint angles move during the rehabilitation training; therefore, the iTbot's forward kinematics analysis and updated Denavit–Hartenberg (DH) [46] parameters are utilized. The iTbot's kinematic model was created using modified DH notations. Each robot connection has a coordinate frame (link frame) connected to it that describes its location in relation to its neighbors. Figure 3 depicts the system's serial link-frame end-effector-type robot attachments.

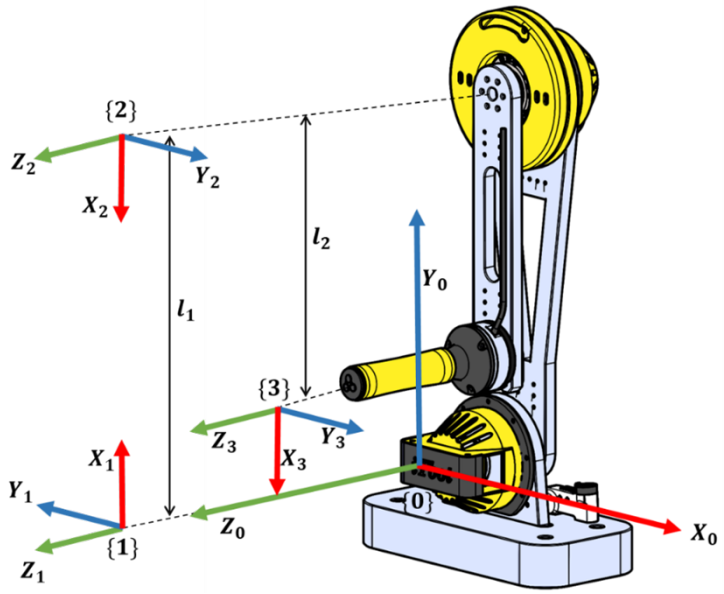

Figure 3. Coordinate frame assignment for 2DoF iTbot.

To calculate the DH parameters, we consider the co-ordinate frames (i.e., link frames that map one axis of rotation to another). This means that Frame 1 is Joint 1, Frame 2 is Joint-2, and Frame 3 is the end-effector position of the iTbot. The fixed reference frame 0 is considered to match with the initial reference frame at the base frame (world frame). Table 2 summarizes the updated DH parameters related to the location of the link frames (in Figure 3). Integrating the DH parameters yields the homogeneous transfer matrix, which defines the positions and orientations of the reference frame regarding the fixed reference frame.

Table 2. Modified Denavit–Hartenberg parameters.

Joint (i)	α_{i-1}	d_i	a_{i-1}	θ_i
1	0	0	0	$\theta_1 + \frac{\pi}{2}$
2	0	0	l_1	$\theta_2 + \pi$
3	0	0	l_2	0

Where α_{i-1} is the link twist, a_{i-1} corresponds to link length, d_i denotes the link offset, and θ_i is the joint angle of the iTbot.

3.2. Dynamics of the iTbot

The dynamics of the iTbot were analyzed (in Figure 4) in order to imitate joint motions in experiments utilizing non-linear control. The motion of bodies under the influence of external forces was calculated using dynamics. A dynamic model for the iTbot was created using the iterative Newton–Euler approach [47].

The dynamic equation for the iTbot can be expressed by Equation (1)

$$\tau = M(\theta)\ddot{\theta} + V(\theta, \dot{\theta}) + G(\theta) + F(\theta, \dot{\theta}) \tag{1}$$

where $\theta \in \Re^2$ denotes a two-vector of generalized coordinates. $M(\theta) \in \Re^{2x2}$, $V(\theta, \dot{\theta}) \in \Re^{2x1}$, $G(\theta) \in \Re^{2x1}$, are, respectively, the symmetric, bounded, inertia matrix, the Coriolis and centrifugal torques,and the gravitational torque. $\tau \in \Re^2$ is the torque input vector and $F(\theta, \dot{\theta}) \in \Re^2$ represents the external disturbances. Further details are provided in Appendix A.

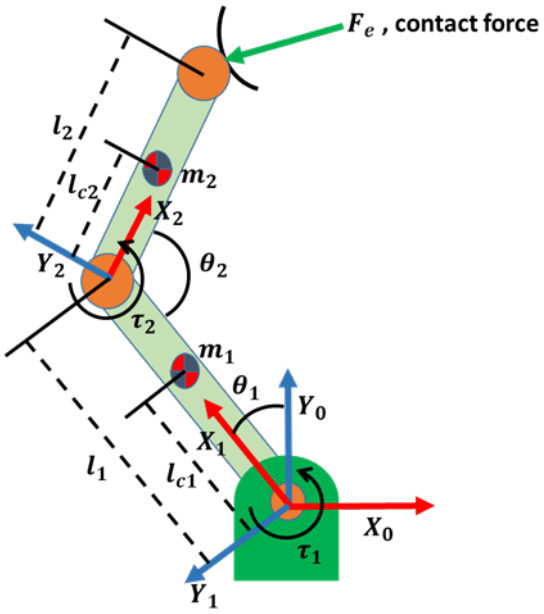

Figure 4. iTbot nomenclature for dynamic modeling with contact force at the end-effector.

4. Control Design and Stability Analysis

Introducing $x = \theta$ and $\dot{x} = \dot{\theta}$, the dynamic model expressed in Equation (1) can be rewritten in the form of Equation (2) as follows:

$$\ddot{x} = f(x, \dot{x}) + g(x)u \tag{2}$$

with:

- $u = \tau$
- $g(x) = g = M^{-1}(\theta)$
- $f(x, \dot{x}) = f = M^{-1}(\theta)\left[-C(\theta, \dot{\theta})\dot{\theta} - G(\theta) - F(\theta, \dot{\theta})\right]$

The tracking position error can be given by: $e = x - x^d$, where $x^d \in \Re^n$ is the reference trajectory and x is the actual position.

The first step in conceiving an SMC approach is to choose the switching surface ν as follows:

$$\nu = \dot{e} + \lambda e \tag{3}$$

where $\lambda \in \Re^{n \times n} > 0$. Note that λ plays a decisive role in the convergence rate of the error tracking to zero.

Consider the Lyapunov function: $V(\nu) = \frac{1}{2}\nu^T\nu$, with its time derivative:

$$\dot{V} = \nu^T\dot{\nu} \tag{4}$$

The criterion for stability is therefore: $\dot{V} < 0$. This requires $\dot{\nu} < 0$ for $\nu > 0$ and $\dot{\nu} > 0$ for $\nu < 0$, which gives rise to the commonly known control law switching phenomenon around $\nu = 0$. Based on (Equation (3)) and its derivative, the following control input is proposed:

$$u = g^{-1}\left[\ddot{x}^d - \lambda\dot{e} - f + \dot{\nu}\right] \tag{5}$$

Note that, from (Equation (5)), the control input is substantially based on $\dot{\nu}$, which in turn defines the rate of ν. So, if $\dot{\nu} \ll 0$ for $\nu > 0$ (with the opposite being too correct), the dynamics' pushed trajectory converges to $\nu = 0$. Therefore, $\dot{\nu}$ is usually referred to as the "reaching" law. When the trajectory of the system is in the vicinity of $\nu = 0$, with $\dot{V} < 0$, $\dot{\nu} < 0$ determines precisely how close the system is to the sliding surface $\nu = 0$. Therefore, a "switching" phenomenon arises in order to maintain the condition: $\nu\dot{\nu} < 0$.

To cope with the high gain value of SMC and to produce rapid and high tracking performance, a kind of adaptive reaching known as the exponential reaching law (ERL) was proposed. This approach is considered to be an effective approach to overcome this issue.

The ERL technique solves the problem associated with the high gain of the SMC reaching law by allowing the controller to dynamically respond to variations in the switching function. This method allows the SMC control gain to be readily varied between an appropriate amount of control gain that does not cause chattering K_{1i} and K_{1i}/ϕ_i where $\phi_i < 1$ (for definition of variables see Equation (6) below). As a result, the ERL approach can guarantee the convergence rate in the period indicated by Equation (7). The fundamental issue with this strategy is that it cannot prevent chattering at the start of motions, which reduces the accuracy of the control performance. The suggested controller was created to overcome this issue, while maintaining the high converge time lower than the ERL. The designed reaching law is defined as follows:

$$\begin{aligned}\dot{\nu}_i = &-\frac{K_{1i}}{\phi_i + (1-\phi_i)e^{-\alpha_i|\nu_i|^{p_i}}}|\nu_i|^{\varphi} sign(\nu_i) \\ &-\omega_i \frac{K_{1i}(1-\varphi)}{\phi_i} sign(\nu_i)\end{aligned} \tag{6}$$

where $\phi_i > 0$, $\alpha_i > 0$ and $p_i > 0$ with $\phi_i < 1$ and $0 < \varphi < 0.5$. ω_i is defined by $\lim_{t\to\infty}(\omega_i) = 0$ and $\int_0^t \omega_i(w)dw = Q_i < \infty$, where $\omega_i = 1/(1+t_i^2)$ and t_i is the execution time of the reference trajectory. The second term of the control law, Equation (6) is designed to preserve its robustness around the beginning of the executing trajectory. Note that, as time goes on, this term would disappear based on the definition of ω_i.

Note that, the term φ is commonly defined as a high value in the classical power rate law to guarantee fast convergence to the origin while causing unwanted chattering. In the designed law, a restriction on φ was imposed: $0 < \varphi < 0.5$. This would guarantee not only fast convergence, but also reduced chattering.

Proposition 1. *For $K_{1i} > 0$, and in conformity with the selection of φ determined in advance, the proposed reaching law (Equation (6)) consistently provides faster convergence to the origin than ERL [42] and ensures stability of the closed loop dynamical system Equation (2).*

Proof. The ERL's reaching time is provided in [42]:

$$Tr_{1i} = \frac{1}{K_i}\left(\phi_i|\nu_i(0)| + (1-\phi_i)\int_0^{|\nu_i(0)|} e^{-\alpha_i|\nu_i|^{p_i}} d\nu_i\right) \tag{7}$$

To obtain the reaching time (Tr_{2i}) of the designed reaching law (6), it is initially rewritten as:

$$dt_i = \frac{\left(\phi_i + (1-\phi_i)e^{-\alpha_i|\nu_i|^{p_i}}\right)d\nu_i}{-K_{1i}|\nu_i|^{\varphi}sign(\nu_i)} + \frac{\phi_i d\nu_i}{-\omega_i K_{1i}(1-\varphi)sign(\nu_i)}. \tag{8}$$

Integrating (Equation (8)) from zero to Tr_{2i}, with $\nu_i(Tr_{2i}=0)$, gives:

$$\begin{aligned} Tr_{2i} &= \int_{\nu_i(0)}^{0} \frac{\left(\phi_i + (1-\phi_i)e^{-\alpha_i|\nu_i|^{p_i}}\right)d\nu_i}{-K_{1i}|\nu_i|^{\varphi}sign(\nu_i)} + \int_{\nu_i(0)}^{0} \frac{\phi_i d\nu_i}{-\omega_i K_{1i}(1-\varphi)sign(\nu_i)}. \\ &= \int_{0}^{\nu_i(0)} \frac{\left(\phi_i + (1-\phi_i)e^{-\alpha_i|\nu_i|^{p_i}}\right)d\nu_i}{K_{1i}|\nu_i|^{\varphi}sign(\nu_i)} + \int_{0}^{\nu_i(0)} \frac{\phi_i d\nu_i}{\omega_i K_{1i}(1-\varphi)sign(\nu_i)}. \end{aligned} \tag{9}$$

if $\nu_i < 0$ for all $ti < Tr_{2i}$, so:

$$Tr_{2i} = \int_{0}^{-\nu_i(0)} \frac{\left(\phi_i + (1-\phi_i)e^{-\alpha_i|\nu_i|^{p_i}}\right)d\nu_i}{K_{1i}|\nu_i|^{\varphi}} + \int_{0}^{-\nu_i(0)} \frac{\phi_i d\nu_i}{\omega_i K_{1i}(1-\varphi)}. \tag{10}$$

Else, if $\nu_i > 0$ for all $ti < Tr_{2i}$, gives:

$$Tr_{2i} = \int_{0}^{\nu_i(0)} \frac{\left(\phi_i + (1-\phi_i)e^{-\alpha_i|\nu_i|^{p_i}}\right)d\nu_i}{K_{1i}|\nu_i|^{\varphi}} + \int_{0}^{\nu_i(0)} \frac{\phi_i d\nu_i}{\omega_i K_{1i}(1-\varphi)}. \tag{11}$$

Based on Equations (10) and (11):

$$Tr_{2i} = \int_{0}^{|\nu_i(0)|} \frac{\phi_i d\nu_i}{K_{1i}|\nu_i|^{\varphi}} + \int_{0}^{|\nu_i(0)|} \frac{(1-\phi_i)e^{-\alpha|\nu_i|^{p_i}}d\nu_i}{K_{1i}|\nu_i|^{\varphi}} + \int_{0}^{|\nu_i(0)|} \frac{\phi_i d\nu_i}{\omega_i K_{1i}(1-\varphi)}. \tag{12}$$

Then:

$$Tr_{2i} = \frac{1}{K_{1i}}\left(\phi_i \frac{|\nu_i(0)|^{(1-\varphi)}}{(1-\varphi)} + \frac{\phi_i|\nu_i(0)|}{\omega_i(1-\varphi)} + (1-\phi_i)\int_{0}^{|\nu_i(0)|} e^{-\alpha_i|\nu_i|^{p_i}}|\nu_i|^{-\varphi}d\nu_i\right). \tag{13}$$

In [42], the authors applied the properties of Euler's gamma function (φ) to demonstrate that the reaching time Tr_{1i} fulfils the next conditions:

$$Tr_{1i} \leq \frac{\phi_i}{K_{1i}}|\nu_i(0)| + \frac{(1-\phi_i)}{K_{1i}\alpha_i^{1/p_i}}. \tag{14}$$

By adopting similar properties of Euler's gamma function for the designed reaching law, the last term of (Equation (13)) can be rewritten in terms of the φ function as:

$$\int_0^{|\nu_i(0)|} e^{-\alpha_i|\nu_i|^{p_i}}|\nu_i|^{-\varphi}d\nu_i = \alpha_i^{\varphi/p_i}\frac{\left[\varphi^-\left(\frac{\varphi-1}{p_i}\right)-\varphi\left(-\left(\frac{\varphi-1}{p_i}\right),\alpha_i|\nu_i(0)|^{p_i}\right)\right]}{p_i\alpha_i^{1/p_i}}. \tag{15}$$

According to the properties of the φ function:

$$\varphi\left(-\left(\frac{\varphi-1}{p_i}\right),\alpha_i|\nu_i(0)|^{p_i}\right) \ll \varphi^-\left(\frac{\varphi-1}{p_i}\right). \tag{16}$$

Thus, it is valid to suppose that: $\varphi\left(-\left(\frac{\varphi-1}{p_i}\right),\alpha_i|\nu_i(0)|^{p_i}\right) \approx 0$, and, hence:

$$\int_0^{|\nu_i(0)|} e^{-\alpha_i|\nu_i|^{p_i}}|\nu_i|^{-\varphi}d\nu_i = \alpha_i^{\varphi/p_i}\frac{\varphi^-\left(\frac{\varphi-1}{p_i}\right)}{p_i\alpha_i^{1/p_i}}. \tag{17}$$

substituting Equation (17) into Equation (13), it is established that the reaching time achieves the following condition:

$$Tr_{2i} \leq \frac{\phi_i}{K_{1i}}\left[\frac{|\nu_i(0)|^{(1-\varphi)}+\omega_i|\nu_i(0)|}{(1-\varphi)}\right] + \left(\frac{1-\phi_i}{K_{1i}}\right)\frac{\varphi^-\left(\frac{\varphi-1}{p_i}\right)}{p_i\alpha_i\left(\frac{1-\varphi}{p_i}\right)} \tag{18}$$

To show that the designed reaching law presents a reaching time shorter than that given by ERL [42], it is important to rewrite the reaching time of the designed law as:

$$Tr_{2di} = \frac{\phi_i}{K_{1i}}\left[\frac{|\nu_i(0)|^{(1-\varphi)}+\omega_i|\nu_i(0)|}{(1-\varphi)}\right] + \left(\frac{1-\phi_i}{K_{1i}}\right)\frac{\varphi^-\left(\frac{\varphi-1}{p_i}\right)}{p_i\alpha_i\left(\frac{1-\varphi}{p_i}\right)}. \tag{19}$$

Thus, the reaching time Tr_{2i} should be lower than the desired reaching time Tr_{2di} for each value of α as:

$$\alpha_i \gg \left[\frac{(1-\phi_i)\varphi^-\left(\frac{\varphi-1}{p_i}\right)(1-\varphi)}{\phi_i\left(|\nu_i(0)|^{(1-\varphi)}+\omega_i|\nu_i(0)|\right)}\right]^{\frac{p_i}{1-\varphi}}. \tag{20}$$

Therefore, the desired reaching law can be re-estimated as:

$$Tr_{2di} \approx \frac{\phi_i}{K_{1i}} \left[\frac{|\nu_i(0)|^{(1-\varphi)} + \omega_i |\nu_i(0)|}{(1-\varphi)} \right]. \tag{21}$$

In addition, the gain K_{1i} should fulfil:

$$K_{1i} \approx \frac{\phi_i}{Tr_{2di}} \left[\frac{|\nu_i(0)|^{(1-\varphi)} + \omega_i |\nu_i(0)|}{(1-\varphi)} \right]. \tag{22}$$

If both condition Equations (20) and (22) are fulfilled, it can then be guaranteed that $Tr_{2i} < Tr_{2di}$. Since the suggested reaching law will be against the ERL [42], it would be advantageous to indicate the desired reaching law, along with the tuning gain, provided by the ERL proposition:

$$Tr_{1di} \approx \phi_i \frac{|\nu_i(0)|}{K_{1i}} \tag{23}$$

$$K_{1i} \approx \phi_i \frac{|\nu_i(0)|}{Tr_{1di}} \tag{24}$$

Subtracting (21) from (23) gives:

$$\begin{aligned} Tr_{1di} - Tr_{2di} &\approx \phi_i \frac{|\nu_i(0)|}{K_{1i}} - \frac{\phi_i}{K_{1i}} \left[\frac{|\nu_i(0)|^{(1-\varphi)} + \omega_i |\nu_i(0)|}{(1-\varphi)} \right] \\ &\approx \frac{\phi_i}{K_{1i}} |\nu_i(0)| \left[1 - \left(\frac{|\nu_i(0)|^{-\varphi} + \omega_i}{(1-\varphi)} \right) \right] \end{aligned} \tag{25}$$

Since $\phi_i > 0$ and $K_{1i} > 0$, it is then obvious that $\frac{\phi_i}{K_{1i}} |\nu_i(0)|$ is always positive.

It is important to demonstrate that the second term of (Equation (25)) is always positive. According to the definition of ω_i in (Equation (6)), as $t \longrightarrow \infty$, the term $\omega_i \longrightarrow 0$. In this case, to prove that the second term of (Equation (25)) is always positive, the next should hold:

$$\frac{1}{|\nu_i(0)|^{\varphi}(1-\varphi)} < 1 \tag{26}$$

which means that the next must hold:

$$|\nu_i(0)| > (1-\varphi)^{-1/\varphi} \tag{27}$$

Therefore,

$$\left(1 - \frac{1}{|\nu_i(0)|^{\varphi}(1-\varphi)} \right) > 0, \forall |\nu_i(0)| > (1-\varphi)^{-1/\varphi} \tag{28}$$

Then, (Equation (25)) can be rewritten as:

$$\begin{aligned} Tr_{1di} - Tr_{2di} \approx \frac{\phi_i}{K_{1i}} |\nu_i(0)| \left[1 - \left(\frac{|\nu_i(0)|^{-\varphi}}{(1-\varphi)} \right) \right] > 0, \\ \forall |\nu_i(0)| > (1-\varphi)^{-1/\varphi} \end{aligned} \tag{29}$$

Note that, according to Equations (18) and (19), $Tr_{2i} \leq Tr_{2di}$. Moreover, based on [42], $Tr_{1i} \leq Tr_{1di}$. Therefore, according to the condition provided by (Equation (29)), the next can be rewritten:

$$Tr_{1i} - Tr_{2i} > 0, \forall |\nu_i(0)| > (1-\varphi)^{-1/\varphi} \tag{30}$$

Thus, based on the value of φ, the reaching time of the designed law is shorter than that given by the ERL. So, the proof is finished. □

5. Experimental and Comparative Study Evaluation

5.1. Real-Time System Setup

Figure 5 depicts the experimental configuration of the iTbot architecture. Three levels of computing units comprise the rehabilitation robot instrumentation system. To communicate with the rehabilitation robot, a user interface (UI) runs on a personal computer (PC). The UI is used to send control and operation commands to the rehabilitation robot, as well as to visualize the live data for joint positioning and force the sensor inputs. The second level of computing is performed in a National Instruments CompactRIO, running as a RealTime target. LabVIEW RealTime applications running in the RealTime target perform the computational tasks of trajectory generation, position control, and feedback processing using the programmed algorithms. The RealTime applications also collect and store data during robot operation and send the data to the UI application on the PC to be saved for analysis. The third level of computing is performed in the field programmable gate array (FPGA) built into the CompactRIO, which runs at 50 µs to run a PI control algorithm to control the motor current and to process hall-sensor signals from the motors to calculate the joint position. The joints of the iTbot rehabilitation robot are powered by Brushless DC (BLDC) motors (Maxon EC-45 Flat, 70 and 30-watt variants) with Harmonic Drive strain wave reducers that provide a 100:1 gear ratio. The motors are driven by ZB12A brushless servo amplifiers. The motor's built-in hall-sensors are used for both commutations by the servo amplifiers and for position feedback by the FPGA system.

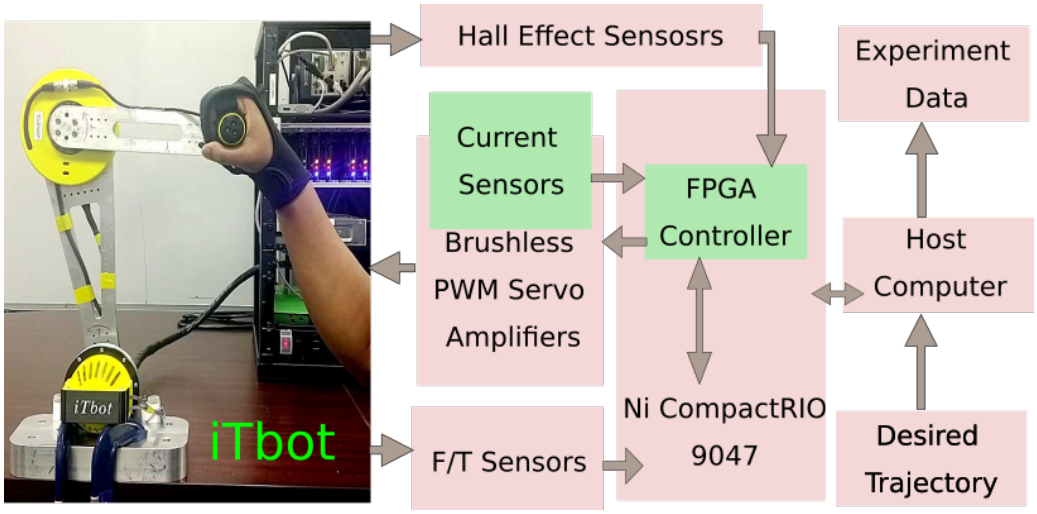

Figure 5. Experimental setup with iTbot architecture.

5.2. Experimental Results

To assess the proposed new sliding mode exponential reaching law (nSMERL), our developed iTbot was deployed to provide passive arm movement exercises to a healthy human subject. Passive arm movement therapy is the first form of physiotherapy treatment that patients receive, aiming to improve their passive range of motion. The proposed nSMERL controller was compared to a SMERL [48] and conventional SMC [38]. Multi-joint movement (desired trajectory) was performed in this experiment, using all of the robot's joints. The purpose of this test was to demonstrate the proposed nSMERL controller's

performance during passive rehabilitation exercises. The proposed nSMERL technique was used to monitor the required motion in the first scenario. In the second scenario, which employed the same individual (age: 28 years; height: 5ft 4 in; Weight: 125 lbs.) and same exercise, the precise target trajectory was tracked using SMERL and a conventional sliding mode controller, which was used to monitor the first. The goal was to demonstrate how the nSMERL controller differed from existing controllers. The individual was seated on a chair that had been adjusted to their comfort level. The controller gain parameters were manually selected by trial and error, as shown in Table 3.

Table 3. Gain parameters.

λ_i	K_i	Φ_i	α_i	P_i	Φ
40	2	0.1	2	0.5	0.25
50	0.8	0.1	2	0.5	0.25

The elimination of chattering is the major improvement achieved by the proposed nSMERL. Chattering causes high-frequency vibration to the mechanical structure, which might cause harm to the participants involved; therefore, it has to be mitigated or eradicated. We carried out a multi-joint rehabilitation exercise to evaluate the efficacy of the proposed nSMERL in reducing chattering. The desired trajectories (reference trajectories, dotted line) were compared to the measured trajectories (solid line) and the tracking error, as shown in Figures 6 and 7. Figure 8 show the joint angles for three controllers. Error, or the difference between the desired and actual trajectories, is shown as a function of time in Figure 9 for both controllers. Figure 10 displays a plot of the joint torques that were created to follow the trajectory; the result demonstrates that the method provided more stable tracking and less chattering than the conventional SMC method. The error plots also show that the proposed SMC outperformed the conventional SMC in terms of tracking accuracy. For example, we sought to keep the higher tracking errors below two degrees for the three controllers.

Figure 11 displays force graphs which show that the additional weight (1lb) applied to participants' hands caused maximum resistive forces of approximately Fx = 14 N and Fy = 10 N. The extra weight cannot precisely simulate spasticity, but it was sufficient to demonstrate that the controller was capable of withstanding patients' spasticity. As a result, despite the fact that the robot's dynamic model and external disturbances were linearized to a simple linear system, the end-effector robot (iTbot) performed satisfactorily under the proposed SMC controller, in comparison to conventional SMC, which retains the non-linear dynamic method in its control strategy. The proposed nSMERL controller continuously provided appropriate tracking with modest control input and less chattering. While the conventional SMC controller produced satisfactory results, its control input was significantly greater than that of the proposed controller (high chattering). These findings demonstrate that the proposed nSMERL controller improved the other sliding mode approach.

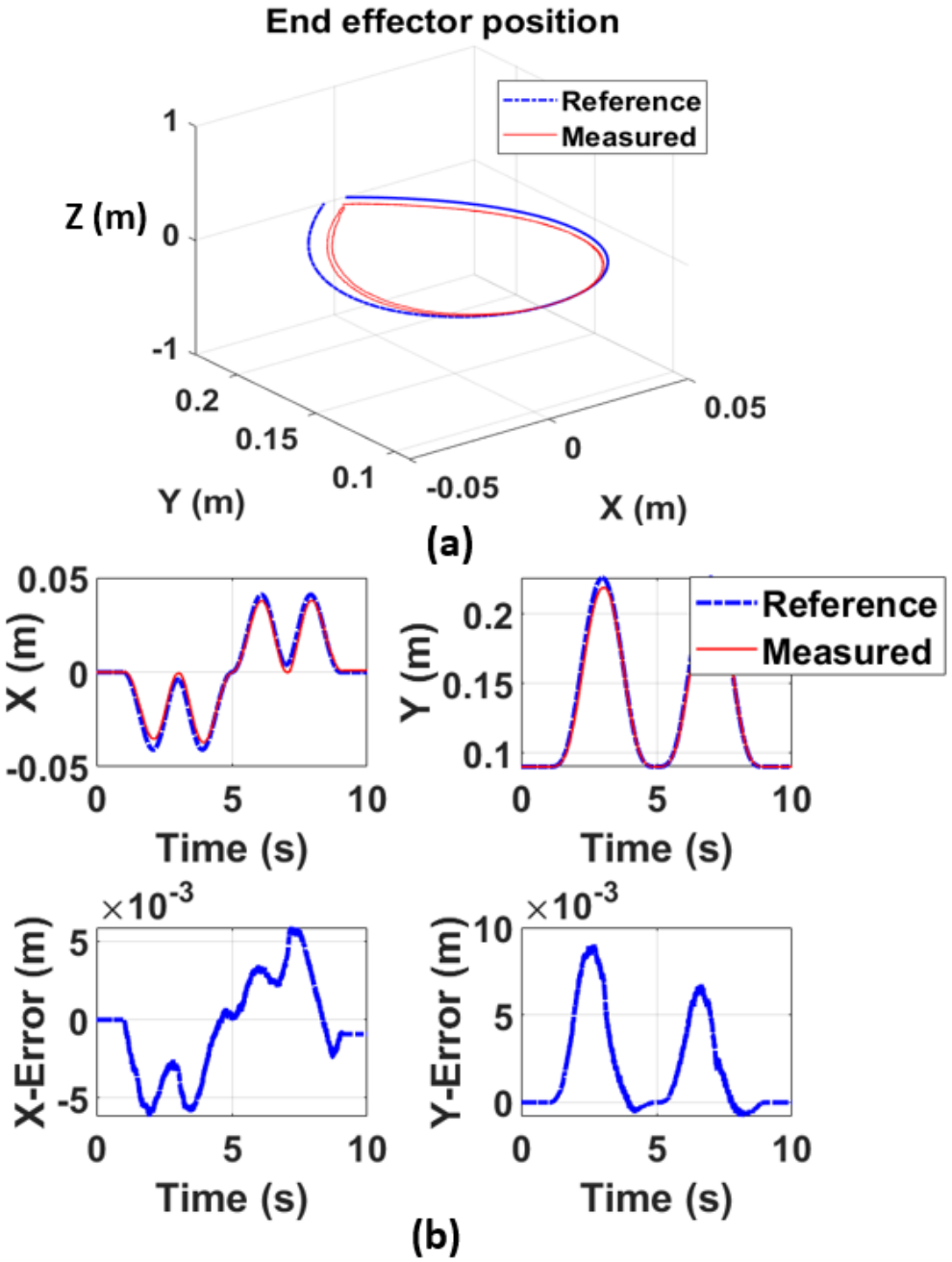

Figure 6. (**a**) End-effector position under the proposed nSMERL, (**b**) End-effector tracking error under the proposed nSMERL.

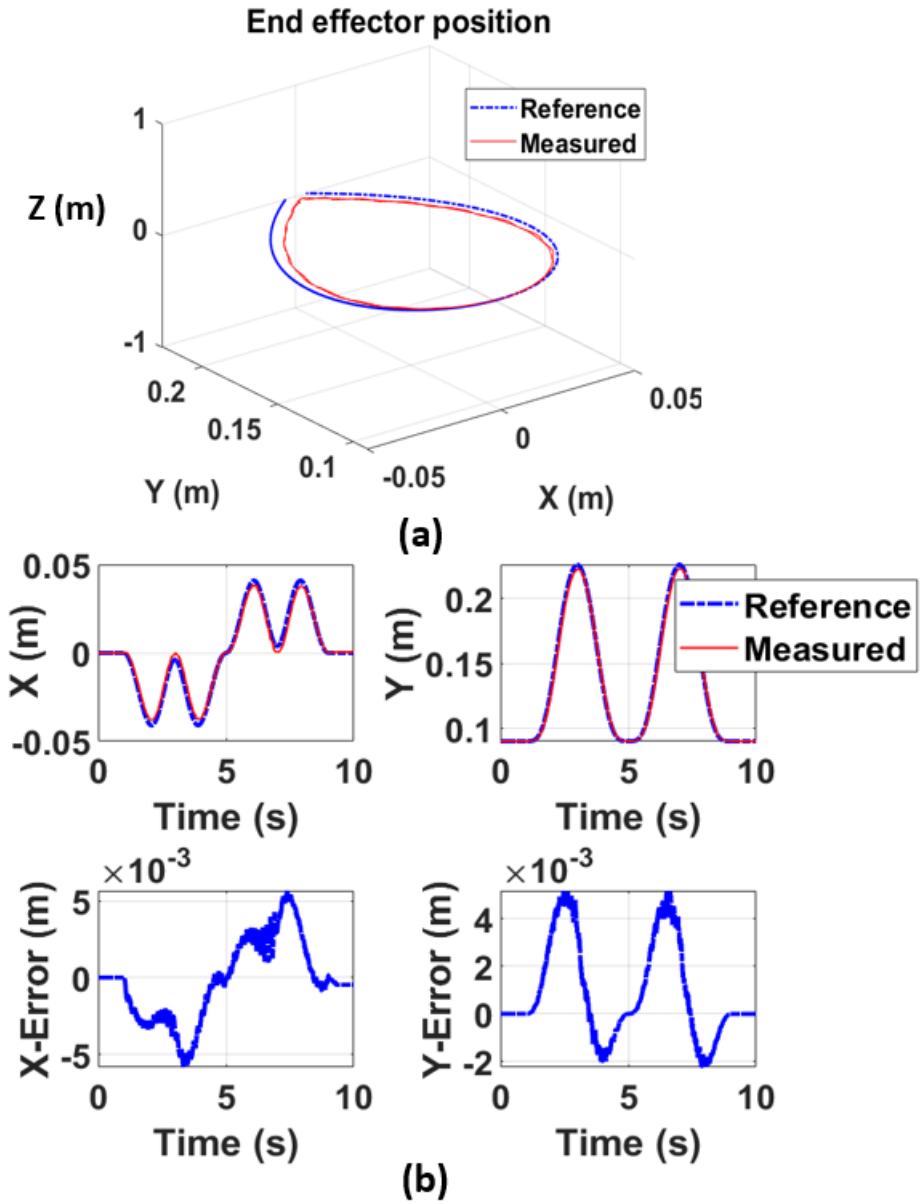

Figure 7. (**a**) End-effector position under the SMERL and conventional SMC, (**b**) End-effector tracking error under the SMERL and conventional SMC.

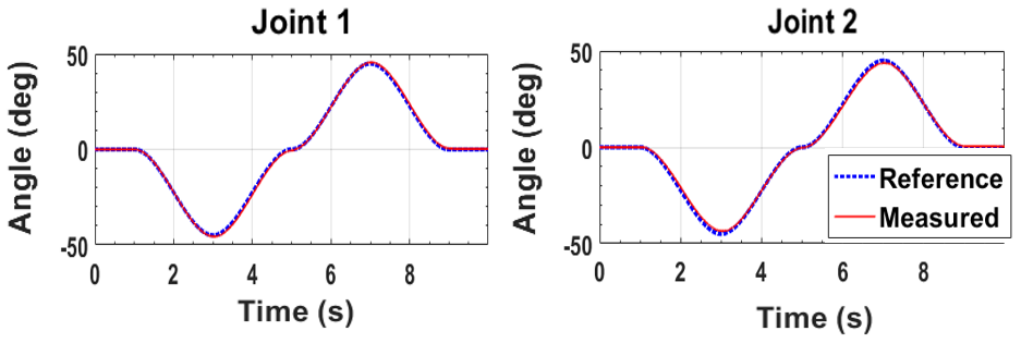

Figure 8. Joint angle for the proposed nSMERL, SMERL, and conventional SMC.

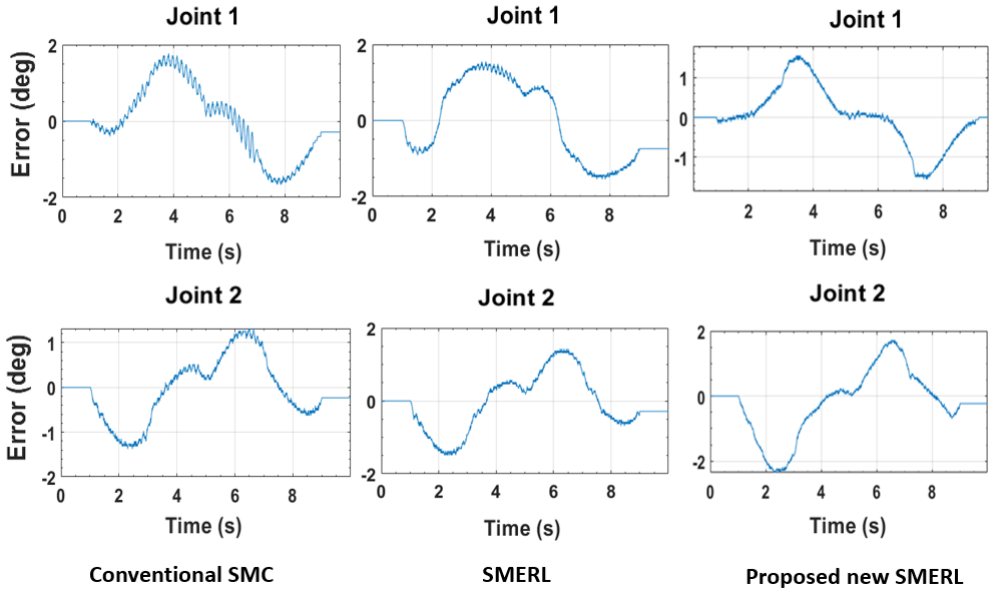

Figure 9. Tracking of joint errors under the proposed nSMERL, SMERL, and conventional SMC.

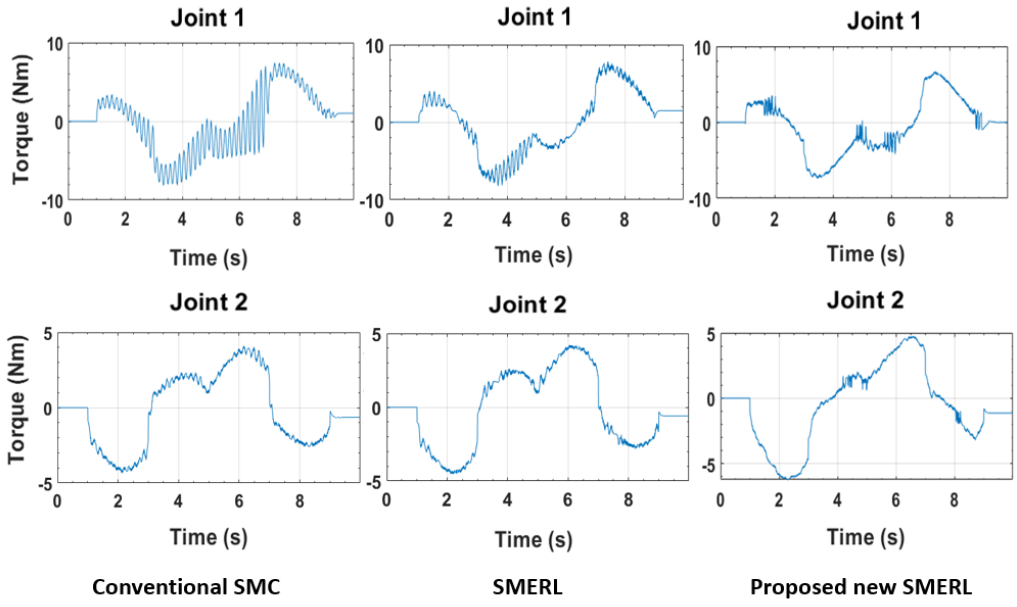

Figure 10. Joint torque for the proposed nSMERL, SMERL, and conventional SMC.

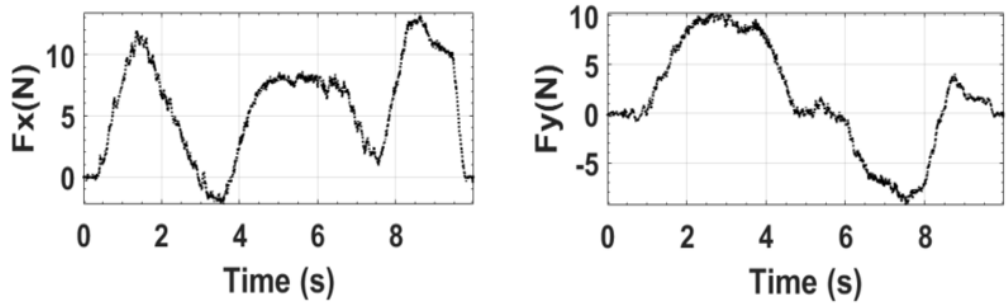

Figure 11. Force (end-effector) data during experiments.

6. Conclusions and Future Work

Robot-assisted treatment has emerged as a valuable technique in the rehabilitation and reinforcement of motor skills in individuals suffering from neuromuscular ailments. An end-effector-type robot was presented to assist in the rehabilitation training of elbow flexion and extension motions. To evaluate the efficacy of the proposed method, multiple trajectory tracking experiments were carried out using a real-time control system. The proposed control law demonstrated its potential to both overcome and improve the performance of SMERL. To evaluate the efficacy of the proposed nSMERL, multiple trajectory tracking experiments were carried out using a real-time control system. The proposed nSMERL, a novel non-linear control approach, enhanced transient tracking performance and decreased chattering in SMERL and conventional SMC. Experiments were conducted to evaluate the dynamic tracking performance of SMERL and conventional SMC with the proposed nSMERL. It was shown that the proposed nSMERL could reduce chattering and provide superior tracking performance. A Kinect sensor will be used in future research to detect the motions of the human arm. A further investigation into EMG signals is planned to achieve more advanced rehabilitation and assistive control.

Author Contributions: Conceptualization, B.B. and M.H.R.; Data curation, M.M.R.K., T.A.; Formal analysis, R.F., M.R.I. and M.H.R.; Investigation, M.R.I. and M.H.R.; Methodology, M.M.R.K., A.A.Z.S.; Software, M.M.R.K., A.A.Z.S., T.A., M.R.I.; Supervision, M.H.R.; Validation, M.M.R.K., B.B. and M.H.R.; Visualization, M.M.R.K., A.A.Z.S.; Writing—original draft, M.M.R.K., B.B., and A.A.Z.S.; Writing—review & editing, M.M.R.K., B.B., M.R.I. and M.M.R. All authors have read and agreed to the published version of the manuscript.

Funding: This research received no external funding.

Data Availability Statement: The data that support the findings of this study are available from the corresponding author, [Md Mahafuzur Rahaman Khan], upon reasonable request.

Acknowledgments: The authors would like to thank Helal Uddin Ahmed for his participation and assistance in finalizing the reviews of this work.

Conflicts of Interest: The authors declare no conflict of interest.

Appendix A

Appendix A.1. Kinematics of the iTbot

The general form of a link transformation that relates the frame i relative to the frame $i-1$ [49] is:

$$ {}^{i-1}_{i}T = \begin{bmatrix} {}^{i-1}_{i}R^{3\times3} & {}^{i-1}_{i}P^{3\times1} \\ 0^{1\times3} & 1 \end{bmatrix} \tag{A1} $$

where, ${}^{i-1}_{i}\mathbf{R}$ is the rotation matrix that represents the frame i relative to frame **i-1** and can be articulated as follows:

$$ {}^{i-1}_{i}R = \begin{bmatrix} \cos\theta_i & -\sin\theta_i & 0 \\ \sin\theta_i\cos\alpha_{i-1} & \cos\theta_i\cos\alpha_{i-1} & -\sin\alpha_{i-1} \\ \sin\theta_i\sin\alpha_{i-1} & \cos\theta_i\sin\alpha_{i-1} & \cos\alpha_{i-1} \end{bmatrix} \tag{A2} $$

and ${}^{i-1}_{i}\mathbf{P}$ is the vector that locates the origin of the frame i relative to frame $i-1$ and can be expressed as the following:

$$ {}^{i-1}_{i}P = \begin{bmatrix} \alpha_{i-1} & -\sin(\alpha_{i-1})d_i & \cos(\alpha_{i-1})d_i \end{bmatrix}^T \tag{A3} $$

The homogenous transformation matrix that relates frame 3 to frame 0 can be obtained by multiplying individual transformation matrices that result in the generic form (A4).

$$ {}^{0}_{3}T = \left[{}^{0}_{1}T \cdot {}^{1}_{2}T \cdot {}^{2}_{3}T \right] \tag{A4} $$

Appendix A.2. Dynamics of the iTbot

Then, the joint torques of the iTbot for vertical configuration with active gravity compensation, based on the nomenclature provided in Figure 4, can be found by the iterative Newton–Euler formulation as:

$$ \begin{aligned} \tau_1 = {} & \left(m_2 l_1^2 - 2m_2 l_1 l_{c2} \cos(\theta_2) + m_1 l_{c1}^2 + m_2 l_{c2}^2 + I_{z1} + I_{z2}\right)\ddot{\theta}_1 \\ & + \left(m_2 l_{c2}^2 - m_2 l_1 l_{c2} \cos(\theta_2) + I_{z2}\right)\ddot{\theta}_2 + m_2 l_1 l_{c2} \sin(\theta_2)\dot{\theta}_2^2 \\ & + 2m_2 l_1 l_{c2} \sin(\theta_2)\dot{\theta}_1\dot{\theta}_2 + \left(m_2 l_{c2} \sin(\theta_1 + \theta_2) - m_1 l_{c1} \sin(\theta_1) - m_2 l_1 \sin(\theta_1)\right) \end{aligned} \tag{A5} $$

$$ \begin{aligned} \tau_2 = {} & \left(I_{z2} + m_2 l_{c2}(l_{c2} - l_1 \cos(\theta_2))\right)\ddot{\theta}_1 \\ & + \left(m_2 l_{c2}^2 + I_{z2}\right)\ddot{\theta}_2 - m_2 l_1 l_{c2} \sin(\theta_2)\dot{\theta}_1^2 + \left(m_2 l_{c2} \sin(\theta_1 + \theta_2)\right) \end{aligned} \tag{A6} $$

where m_1, m_2 is the mass of Link 1 and Link 2; l_{c1} is the distance relative to 1 and center of mass (Link 1), l_{c1} is the distance relative to 2 and center of mass (Link 2); l_1, l_2 is the length of Link 1 and Link 2; I_{z1}, I_{z2} is the inertia tensor ; τ_1, τ_2 is the inertia of Joint 1 and Joint 2.

Equations (A5) and (A6) give expressions for the torque at the actuators as a function of joint position, velocity, and acceleration. The dynamic Equation of iTbot can be written in the form given by Equation (A7):

$$ \tau = M(\theta)\ddot{\theta} + V\left(\theta, \dot{\theta}\right) + G(\theta) \tag{A7} $$

where and are the 2 × 1 torque and acceleration vector. $M(\theta)$ is the 2 × 2 mass matrix given as:

$$ M(\theta) = \begin{bmatrix} \kappa_1 & \kappa_2 \\ I_{z2} + m_2 l_{c2}(l_{c2} - l_1 \cos(\theta_2)) & m_2 l_{c2}^2 + I_{z2} \end{bmatrix} \tag{A8} $$

where κ_1 and κ_2 are as follows
$\kappa_1 = m_2 l_1^2 - 2m_2 l_1 l_{c2} \cos(\theta_2) + m_1 l_{c1}^2 + m_2 l_{c2}^2 + I_{z1} + I_{z2}$
$\kappa_2 = m_2 l_{c2}^2 - m_2 l_1 l_{c2} \cos(\theta_2) + I_{z2}$

$V\left(\theta, \dot{\theta}\right)$ is a 2 × 1 vector of centrifugal and Coriolis terms given as:

$$ V\left(\theta, \dot{\theta}\right) = \begin{bmatrix} m_2 l_1 l_{c2} \sin(\theta_2)\dot{\theta}_2^2 \cdots \\ \cdots + 2m_2 l_1 l_{c2} \sin(\theta_2)\dot{\theta}_1\dot{\theta}_2 \\ -m_2 l_1 l_{c2} \sin(\theta_2)\dot{\theta}_1^2 \end{bmatrix} \tag{A9} $$

$G(\theta)$ is a 2 × 1 vector of gravity terms given as:

$$ G(\theta) = \begin{bmatrix} (m_2 l_{c2} \sin(\theta_1 + \theta_2) - m_1 l_{c1} \sin(\theta_1) \cdots \\ \cdots - m_2 l_1 \sin(\theta_1))g \\ (m_2 l_{c2} \sin(\theta_1 + \theta_2))g \end{bmatrix} \tag{A10} $$

If $F\left(\theta, \dot{\theta}\right) \in \Re^2$ is the vector of non-linear Coulomb friction and expressed by Equation (A12).

$$ F\left(\theta, \dot{\theta}\right) = c.sgn\left(\dot{\theta}\right). \tag{A11} $$

Then, when friction is added to the model, Equation (A7) becomes Equation (A12):

$$ \tau = M(\theta)\ddot{\theta} + V\left(\theta, \dot{\theta}\right) + G(\theta) + F\left(\theta, \dot{\theta}\right) \tag{A12} $$

References

1. National Spinal Cord Injury Statistical Center. *Facts and Figures at a Glance*; University of Alabama at Birmingham: Birmingham, AL, USA, 2016; Volume 10.
2. Burns, M.; Zavoda, Z.; Nataraj, R.; Pochiraju, K.; Vinjamuri, R. HERCULES: A Three Degree-of-Freedom Pneumatic Upper Limb Exoskeleton for Stroke Rehabilitation. In Proceedings of the 2020 42nd Annual International Conference of the IEEE Engineering in Medicine & Biology Society (EMBC), Montreal, QC, Canada, 20–24 July 2020; pp. 4959–4962.
3. Mackay, J.; Mensah, G.A.; Greenlund, K. *The Atlas of Heart Disease and Stroke*; World Health Organization: Geneva, Switzerland, 2004.
4. Johnson, W.; Onuma, O.; Owolabi, M.; Sachdev, S. Stroke: A global response is needed. *Bull. World Health Organ.* **2016**, *94*, 634.
5. Hatem, S.M.; Saussez, G.; Della Faille, M.; Prist, V.; Zhang, X.; Dispa, D.; Bleyenheuft, Y. Rehabilitation of motor function after stroke: A multiple systematic review focused on techniques to stimulate upper extremity recovery. *Front. Hum. Neurosci.* **2016**, *10*, 442.
6. Lawrence, E.S.; Coshall, C.; Dundas, R.; Stewart, J.; Rudd, A.G.; Howard, R.; Wolfe, C.D. Estimates of the prevalence of acute stroke impairments and disability in a multiethnic population. *Stroke* **2001**, *32*, 1279–1284.
7. Nichols-Larsen, D.S.; Clark, P.; Zeringue, A.; Greenspan, A.; Blanton, S. Factors influencing stroke survivors' quality of life during subacute recovery. *Stroke* **2005**, *36*, 1480–1484.
8. Liu, F.; Han, X.; Lin, M.; Wu, X.; Sun, Q.; Song, A. Remote Upper Limb Exoskeleton Rehabilitation Training System Based on Virtual Reality. In Proceedings of the 2019 16th International Conference on Ubiquitous Robots (UR), Jeju, Korea, 24–27 June 2019; pp. 323–327.
9. Bai, J.; Song, A.; Xu, B.; Nie, J.; Li, H. A novel human-robot cooperative method for upper extremity rehabilitation. *Int. J. Soc. Robot.* **2017**, *9*, 265–275.
10. Khan, M.M.R.; Ahmed, T.; Pallares, J.R.H.; Islam, M.R.; Brahmi, B.; Rahman, M.H. Development of A Desktop-mounted Rehabilitation Robot For Upper Extremities. In Proceedings of the International Conference on Industrial & Mechanical Engineering and Operations Management Dhaka, Bangladesh, 26–27 December 2021.
11. Masiero, S.; Armani, M.; Rosati, G. Upper-limb robot-assisted therapy in rehabilitation of acute stroke patients: Focused review and results of new randomized controlled trial. *J. Rehabil. Res. Dev.* **2011**, *48*, 355–366.
12. Duret, C.; Courtial, O.; Grosmaire, A.G.; Hutin, E. Use of a robotic device for the rehabilitation of severe upper limb paresis in subacute stroke: Exploration of patient/robot interactions and the motor recovery process. *BioMed Res. Int.* **2015**, *2015*, 482389.
13. Cao, W.; Chen, C.; Hu, H.; Fang, K.; Wu, X. Effect of hip assistance modes on metabolic cost of walking with a soft exoskeleton. *IEEE Trans. Autom. Sci. Eng.* **2020**, *18*, 426–436.
14. Lim, G.H.; Suh, I.H.; Suh, H. Ontology-based unified robot knowledge for service robots in indoor environments. *IEEE Trans. Syst. Man Cybern.-Part A Syst. Humans* **2010**, *41*, 492–509.
15. Proietti, T.; Crocher, V.; Roby-Brami, A.; Jarrasse, N. Upper-limb robotic exoskeletons for neurorehabilitation: A review on control strategies. *IEEE Rev. Biomed. Eng.* **2016**, *9*, 4–14.
16. Gassert, R.; Dietz, V. Rehabilitation robots for the treatment of sensorimotor deficits: A neurophysiological perspective. *J. Neuroeng. Rehabil.* **2018**, *15*, 1–15.
17. Loureiro, R.C.; Harwin, W.S.; Nagai, K.; Johnson, M. Advances in upper limb stroke rehabilitation: A technology push. *Med. Biol. Eng. Comput.* **2011**, *49*, 1103–1118.
18. Nef, T.; Guidali, M.; Riener, R. ARMin III–arm therapy exoskeleton with an ergonomic shoulder actuation. *Appl. Bionics Biomech.* **2009**, *6*, 127–142.
19. Rahman, M.H.; Rahman, M.J.; Cristobal, O.; Saad, M.; Kenné, J.P.; Archambault, P.S. Development of a whole arm wearable robotic exoskeleton for rehabilitation and to assist upper limb movements. *Robotica* **2015**, *33*, 19–39.
20. Kim, B.; Deshpande, A.D. An upper-body rehabilitation exoskeleton Harmony with an anatomical shoulder mechanism: Design, modeling, control, and performance evaluation. *Int. J. Robot. Res.* **2017**, *36*, 414–435.
21. Zhang, L.; Guo, S.; Sun, Q. Development and assist-as-needed control of an end-effector upper limb rehabilitation robot. *Appl. Sci.* **2020**, *10*, 6684.
22. Nef, T.; Mihelj, M.; Kiefer, G.; Perndl, C.; Muller, R.; Riener, R. ARMin-Exoskeleton for arm therapy in stroke patients. In Proceedings of the 2007 IEEE 10th International Conference on Rehabilitation Robotics, Noordwijk, The Netherlands, 13–15 June 2007; pp. 68–74.
23. Chang, J.J.; Tung, W.L.; Wu, W.L.; Huang, M.H.; Su, F.C. Effects of robot-aided bilateral force-induced isokinetic arm training combined with conventional rehabilitation on arm motor function in patients with chronic stroke. *Arch. Phys. Med. Rehabil.* **2007**, *88*, 1332–1338.
24. Liu, L.; Shi, Y.Y.; Xie, L. A novel multi-dof exoskeleton robot for upper limb rehabilitation. *J. Mech. Med. Biol.* **2016**, *16*, 1640023.
25. Pignolo, L.; Dolce, G.; Basta, G.; Lucca, L.; Serra, S.; Sannita, W. Upper limb rehabilitation after stroke: ARAMIS a "robo-mechatronic" innovative approach and prototype. In Proceedings of the 2012 4th IEEE RAS & EMBS International Conference on Biomedical Robotics and Biomechatronics (BioRob), Rome, Italy, 24–27 June 2012; pp. 1410–1414.
26. Pan, H.; Chen, G.; Kang, Y.; Wang, H. Design and Kinematic Analysis of a Flexible-Link Parallel Mechanism With a Spatially Quasi-Translational End Effector. *J. Mech. Robot.* **2021**, *13*, 011022.

27. Zhao, P.; Zhang, Y.; Guan, H.; Deng, X.; Chen, H. Design of a Single-Degree-of-Freedom Immersive Rehabilitation Device for Clustered Upper-Limb Motion. *J. Mech. Robot.* **2021**, *13*, 031006.
28. Burgar, C.G.; Lum, P.S.; Scremin, A.; Garber, S.L.; Van der Loos, H.; Kenney, D.; Shor, P. Robot-assisted upper-limb therapy in acute rehabilitation setting following stroke: Department of Veterans Affairs multisite clinical trial. *J. Rehabil. Res. Dev.* **2011**, *48*, 445–458.
29. Rahman, M.H.; Saad, M.; Kenné, J.P.; Archambault, P.S. Nonlinear sliding mode control implementation of an upper limb exoskeleton robot to provide passive rehabilitation therapy. In Proceedings of the International Conference on Intelligent Robotics and Applications, Montreal, QC, Canada, 3–5 October 2012; pp. 52–62.
30. Wu, Q.; Chen, B.; Wu, H. Rbfn-based adaptive backstepping sliding mode control of an upper-limb exoskeleton with dynamic uncertainties. *IEEE Access* **2019**, *7*, 134635–134646.
31. Feng, Y.; Zhou, M.; Zheng, X.; Han, F. Continuous adaptive terminal sliding-mode control. In Proceedings of the 2016 IEEE 11th Conference on Industrial Electronics and Applications (ICIEA), Hefei, China, 5–7 June 2016; pp. 184–188.
32. Brahmi, B.; Ahmed, T.; Elbojairami, I.; Swapnil, A.A.Z.; Assaduzzaman, M.; Schultz, K.; Mcgonigle, E.; Rahman, M.H. Flatness Based Control of a Novel Smart Exoskeleton Robot. *IEEE/ASME Trans. Mechatron.* **2021**, *27*, 974–984.
33. Rahman, M.H.; Ochoa-Luna, C.; Saad, M. EMG based control of a robotic exoskeleton for shoulder and elbow motion assist. *J. Autom. Control Eng.* **2015**, *3*, 270–276.
34. Ayas, M.S.; Altas, I.H. Fuzzy logic based adaptive admittance control of a redundantly actuated ankle rehabilitation robot. *Control Eng. Pract.* **2017**, *59*, 44–54.
35. Chen, Z.; Li, Z.; Chen, C.P. Disturbance observer-based fuzzy control of uncertain MIMO mechanical systems with input nonlinearities and its application to robotic exoskeleton. *IEEE Trans. Cybern.* **2016**, *47*, 984–994.
36. Fallaha, C.; Saad, M.; Ghommam, J.; Kali, Y. Sliding mode control with model-based switching functions applied on a 7-dof exoskeleton arm. *IEEE/ASME Trans. Mechatron.* **2020**, *26*, 539–550.
37. Brahmi, B.; Laraki, M.H.; Brahmi, A.; Saad, M.; Rahman, M.H. Improvement of sliding mode controller by using a new adaptive reaching law: Theory and experiment. *ISA Trans.* **2020**, *97*, 261–268.
38. Utkin, V.; Poznyak, A.; Orlov, Y.; Polyakov, A. Conventional and high order sliding mode control. *J. Frankl. Inst.* **2020**, *357*, 10244–10261.
39. Islam, M.R.; Rahmani, M.; Rahman, M.H. A novel exoskeleton with fractional sliding mode control for upper limb rehabilitation. *Robotica* **2020**, *38*, 2099–2120.
40. Babaiasl, M.; Goldar, S.N.; Barhaghtalab, M.H.; Meigoli, V. Sliding mode control of an exoskeleton robot for use in upper-limb rehabilitation. In Proceedings of the 2015 3rd RSI International Conference on Robotics and Mechatronics (ICROM), Tehran, Iran, 7–9 October 2015; pp. 694–701.
41. Khalil, H. Chapter 13: State Feedback Stabilization. *Nonlinear Systems*, 3rd ed.; Prentice Hall: Upper Saddle River, NJ, USA, 2002; pp. 197–227.
42. Fallaha, C.J.; Saad, M.; Kanaan, H.Y.; Al-Haddad, K. Sliding-mode robot control with exponential reaching law. *IEEE Trans. Ind. Electron.* **2010**, *58*, 600–610.
43. Chen, Y.; Fan, J.; Zhu, Y.; Zhao, J.; Cai, H. A passively safe cable driven upper limb rehabilitation exoskeleton. *Technol. Health Care* **2015**, *23*, S197–S202.
44. Ahmed, T.; Islam, M.R.; Brahmi, B.; Rahman, M.H. Robustness and Tracking Performance Evaluation of PID Motion Control of 7 DoF Anthropomorphic Exoskeleton Robot Assisted Upper Limb Rehabilitation. *Sensors* **2022**, *22*, 3747.
45. Lauretti, C.; Cordella, F.; Guglielmelli, E.; Zollo, L. Learning by demonstration for planning activities of daily living in rehabilitation and assistive robotics. *IEEE Robot. Autom. Lett.* **2017**, *2*, 1375–1382.
46. Xiao, F.; Gao, Y.; Wang, Y.; Zhu, Y.; Zhao, J. Design of a wearable cable-driven upper limb exoskeleton based on epicyclic gear trains structure. *Technol. Health Care* **2017**, *25*, 3–11.
47. Luh, J.Y.; Walker, M.W.; Paul, R.P. On-line computational scheme for mechanical manipulators. *J. Dyn. Syst. Meas. Control* **1980**, *102*, 69–76.
48. Rahman, M.H.; Saad, M.; Kenné, J.P.; Archambault, P.S. Control of an exoskeleton robot arm with sliding mode exponential reaching law. *Int. J. Control Autom. Syst.* **2013**, *11*, 92–104.
49. Perry, J.C.; Rosen, J.; Burns, S. Upper-limb powered exoskeleton design. *IEEE/ASME Trans. Mechatron.* **2007**, *12*, 408–417.